ISSN 2072-5981
doi: 10.26907/mrsej

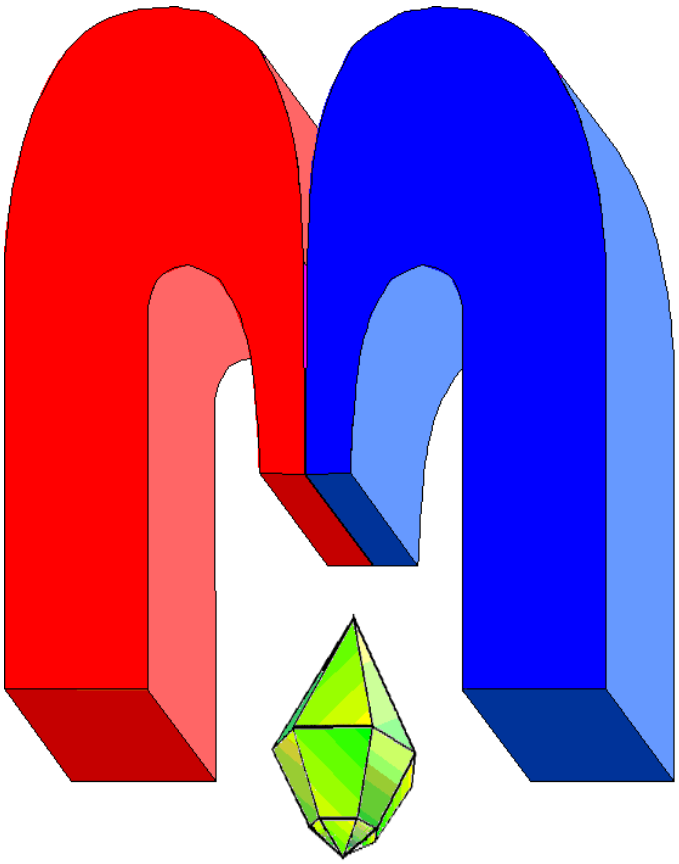

Magnetic Resonance in Solids

Electronic Journal

Volume 27
Issue 3
Article No ***25308***
1-7 pages
2025
doi: **10.26907/mrsej-25308**

http://mrsej.kpfu.ru
http://mrsej.ksu.ru
http://mrsej.elpub.ru

Established and published by Kazan University*
Endorsed by International Society of Magnetic Resonance (ISMAR)
Registered by Russian Federation Committee on Press (#015140), August 2, 1996
First Issue appeared on July 25, 1997

"***Magnetic Resonance in Solids. Electronic Journal***" (**MRS*ej***) is a peer-reviewed, all electronic journal, publishing articles which meet the highest standards of scientific quality in the field of basic research of a magnetic resonance in solids and related phenomena.

Indexed and abstracted by
Web of Science (*ESCI*, Clarivate Analytics, from 2015), *Scopus* (Elsevier, from 2012), *RusIndexSC* (*eLibrary*, from 2006), *Google Scholar*, *DOAJ*, *ROAD*, *CyberLeninka* (from 2006), *SCImago Journal & Country Rank*, etc.

Guest Editor‡: *Marat Gafurov (KFU, Kazan)*

---

* Address: "Magnetic Resonance in Solids. Electronic Journal", Kazan Federal University; Kremlevskaya str., 18; Kazan 420008, Russia

† In Kazan University the Electron Paramagnetic Resonance (EPR) was discovered by Zavoisky E.K. in 1944.

‡ This paper was selected at the International Conference "Modern Development of Magnetic Resonance 2025", September 29 -- October 3, 2025, Kazan, Russia.

Short cite this: *Magn. Reson. Solids* **27**, 25308 (2025) doi: 10.26907/mrsej-25308

Anisotropy of the Magnetic Properties of $GdTiO_3$ Single Crystal†

R. Batulin[1,*], M. Cherosov[1], V. Shustov[2], M. Kuznetcov[1], D. Uvin[1], I. Romanova[1]

[1]Kazan Federal University, Kazan 420008, Russia

[2]Zavoisky Physical-Technical Institute, FRC Kazan Scientific Center of RAS, Kazan 420029, Russia

**E-mail: tokamak@yandex.ru*

(received November 22, 2025; revised December 6, 2025; accepted December 8, 2025; published December 12, 2025)

$GdTiO_3$ is a prototypical Mott-insulating perovskite that exhibits a rich interplay between spin, orbital, and lattice degrees of freedom. Here we report a systematic study of the magnetic anisotropy of high-quality $GdTiO_3$ single crystal grown by the optical floating-zone technique. Comprehensive magnetization measurements performed with a vibrating-sample magnetometer ($5\,\mathrm{K} \le \mathrm{T} \le 70\,\mathrm{K}$, $|\mu_0 H| \le 9\,\mathrm{T}$) reveal a pronounced magnetic anisotropy. The ordering temperature is isotropic ($T_\mathrm{N} \approx 32\,\mathrm{K}$), but both the magnetic susceptibility and the spin-flop fields depend strongly on the direction of the applied field ($H \parallel a, b, c$). For each crystallographic orientation three distinct magnetic regimes are identified: ferromagnetic-like low-field phase, ferrimagnetic high-field phase and paramagnetic phase. These findings provide a solid experimental benchmark for theoretical treatments of spin-orbit coupling and anisotropic exchange in rare-earth titanates. Moreover, the sizable magnetic entropy change associated with the field-driven transitions suggests that $GdTiO_3$ could be exploited in solid-state cryogenic refrigeration based on the magnetocaloric effect, offering a potential route to more efficient hydrogen liquefaction.

PACS: 75.30.Gw, 75.47.Lx, 75.50.Ee

Keywords: rare-earth titanates, magnetic anisotropy, crystal growth, magnetization, $GdTiO_3$

1. Introduction

Rare-earth titanates $R\mathrm{TiO_3}$ (R = La, Nd, Sm, Gd, ...) belong to the family of orthorhombically distorted perovskites (*Pbnm* or *Pnma* space groups) that are canonical examples of Mott–Hubbard insulators with strong electron-correlation effects [1–3]. In these compounds the Ti^{3+} ions ($3d^1$, t_{2g}^1) carry a single electron that is coupled to the localized $4f$ moments of the rare-earth ion [4, 5]. The competition between super-exchange, spin–orbit coupling, and crystal-field effects gives rise to a variety of magnetic ground states, ranging from G-type antiferromagnetism (AFM) in $LaTiO_3$ to ferromagnetism (FM) in $YTiO_3$ [2, 6, 7]. The magnetic properties of this series are governed by the $GdFeO_3$-type octahedral tilts, which modify the Ti–O–Ti bond angles and consequently tune the superexchange interaction according to the Goodenough–Kanamori–Anderson rules [8–10].

$GdTiO_3$ occupies a pivotal position in this series: the Gd^{3+} ion ($4f^7$, $S = 7/2$) provides a large localized moment that couples to the Ti^{3+} sublattice, leading to a complex magnetic ordering below $T_\mathrm{N} \approx 32\,\mathrm{K}$ [1, 4, 5]. Earlier studies identified $GdTiO_3$ as a ferrimagnet, where the Ti sublattice orders ferromagnetically and couples antiferromagnetically to the Gd sublattice [1, 11]. Thin-film investigations have demonstrated that epitaxial strain can substantially modify the magnetic ground state, enabling transitions between ferromagnetic and antiferromagnetic configurations [4, 6, 7]. Recent first-principles calculations have predicted strain-driven sequential

†his paper was selected at the International Conference "Modern Development of Magnetic Resonance 2025", September 29 – October 3, 2025, Kazan, Russia. The guest Editor, Prof. M.R. Gafurov, was responsible for the publication, which was reviewed according to the standard MRSej procedure.

magnetic transitions in $GdTiO_3$ films grown on compressive substrates [7, 8]. Nevertheless, the detailed anisotropic magnetic response of bulk single crystals has remained poorly characterized, mainly because of the difficulty in obtaining large, strain-free single crystals [5, 11, 12].

Understanding magnetic anisotropy is essential for two reasons. First, it directly reflects the underlying exchange pathways and the symmetry of the crystal field, thus providing a stringent test for theoretical models of spin–orbital coupling in titanates [8, 9, 13]. The orthorhombic distortion characteristic of $RTiO_3$ perovskites lifts the orbital degeneracy of the Ti $3d$ t_{2g} states and establishes orbital ordering that dictates the magnetic superexchange [9, 10, 14]. Second, anisotropic magnetic properties are a prerequisite for potential applications in spintronic devices where directional control of magnetization is required [4, 15, 16]. The Dzyaloshinskii–Moriya interaction, permitted by the lack of inversion symmetry at the tilted Ti–O–Ti bonds, can additionally induce weak ferromagnetism and influence domain structures [13, 16].

From a technological standpoint, $GdTiO_3$ has attracted attention as a promising cryogenic magnetocaloric material due to the large magnetic moment of Gd^{3+} and its second-order magnetic transition [5, 17]. The magnetocaloric effect in single crystals was recently characterized, demonstrating the suitability of $GdTiO_3$ for solid-state magnetic refrigeration applications targeting hydrogen liquefaction temperatures. Detailed knowledge of the anisotropic magnetic behavior is therefore critical not only for fundamental physics but also for optimizing magnetocaloric performance.

The optical floating-zone method has proven to be a powerful technique for growing high-quality perovskite oxide single crystals, including related titanates [12, 18, 19]. This crucible-free approach minimizes contamination and allows the synthesis of centimeter-scale boules with low defect densities. Successful growth of stoichiometric $RTiO_3$ requires careful control of oxygen partial pressure to maintain the Ti^{3+} valence state [12, 18]. The question of electron localization versus itinerancy in the Ti $3d^1$ band has been extensively debated, with evidence pointing toward localized behavior stabilized by the $GdFeO_3$-type distortion [19, 20].

In this work we present a comprehensive investigation of the magnetic anisotropy of $GdTiO_3$ single crystals. By employing a high-temperature optical floating-zone furnace we have grown centimeter-scale, untwinned crystals. Magnetization measurements performed with a VSM over a broad temperature (5–70 K) and field (0–9 T) range enable us to determine the main three magnetic phase regions. The results are discussed in the context of anisotropic exchange, crystal-field splitting of the Gd^{3+} ion, and the role of the TiO_6 octahedral tilts.

2. Experimental Methods

2.1. Crystal Growth

Polycrystalline $GdTiO_3$ was synthesized by solid-state reaction using Gd_2O_3 (99.99%), TiO_2 (99.99%), and Ti (99.5%) powders as precursors. The stoichiometric mixture was thoroughly grounded and mixed in an agate mortar. The resulting powder was pressed into a cylindrical rod with diameter approximately 6–7 mm using a hydrostatic press. The rod was installed as the feed rod in a four-mirror optical floating-zone furnace (Crystal Systems Inc.) equipped with 1 kW halogen lamps. Typical growth rate was approximately 10 mm h^{-1}. The detailed growth procedure is beyond the scope of this article and will be published elsewhere. The resulting boules were translucent, black, and free of visible cracks.

2.2. Sample Preparation

Rectangular sample (typical dimensions $2 \times 2 \times 3\,\mathrm{mm}^3$) was cut from the boule using a wire saw and oriented by single-crystal diffraction such that the long edge coincided with the c crystallographic axis. Surfaces were polished with fine alumina slurry to remove any damaged layer. The mass of the sample was 123.0 mg, measured with a microbalance (± 0.01 mg).

2.3. Magnetometry

Magnetization measurements were performed on a Quantum Design Physical Property Measurement System (PPMS) equipped with a vibrating-sample magnetometer (VSM) option. The temperature range covered 5–70 K, and magnetic fields up to 9 T were applied along the selected crystal axis. The procedure was repeated for the three axes.

Temperature dependencies of magnetization were measured in two regimes: zero-field-cooled (ZFC) and field-cooled (FC). In a ZFC regime the sample was cooled from 300 K to 5 K in zero field, after which a static magnetic field, $B = \mu_0 H$, of 0.01 T and 0.1 T was applied and the magnetization was measured as a function of temperature during warming. Data in an FC regime were obtained during warming after cooling the sample in the same applied field. Isothermal magnetization dependencies on external magnetic field were measured: at selected temperatures (5, 25 K), the magnetic field was swept between -9 and $+9$ T at a rate of $0.01\,\mathrm{T\,s^{-1}}$.

3. Results

3.1. Structural Characterization

The phase purity of the samples was previously studied in Ref. [5] using powder X-ray diffraction (Cu K_α) on crushed crystal fragments. The analysis confirmed the single-phase orthorhombic *Pnma* structure with lattice parameters $a = 5.70$ Å, $b = 7.66$ Å, and $c = 5.40$ Å at room temperature. The *Pnma* space group describes the same crystal structure and symmetry as *Pbnm* (space group No. 62), but with a different arrangement of the unit cell axes. No impurity phases were detected within the sensitivity limit ($< 0.5\%$).

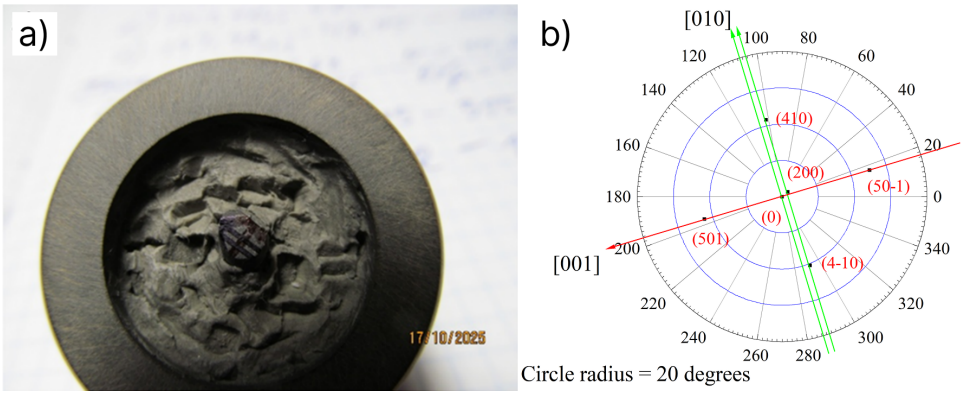

Figure 1. (a) Sample preparation for single-crystal orientation procedure and (b) Stereographic projection of X-ray diffraction data for single-crystal orientation verification and structural quality confirmation.

To verify the quality and orientation of the single crystal used in this work, a specific X-ray diffraction procedure was employed (Fig. 1b). First, the crystal was cut along the (010) plane, perpendicular to the b-axis, with an accuracy better than 1 degree. The orientation was determined by locating reflections from the $(hk0)$ and $(0kl)$ crystallographic planes. During this

procedure, the diffractometer detector was fixed at the 2θ angle corresponding to the specific $(hk0)$ or $(0kl)$ reflection, while the sample was rotated in its own plane (azimuthal rotation around the b-axis). The projections of the scattering vectors perpendicular to these planes onto the polished crystal surface indicated the directions of the a-axis and c-axis, respectively.

This method confirmed the orthorhombic $Pnma$ orientation and the absence of twinning. The deviation of the b-axis from the surface normal was found to be approximately 1 degree. The a- and c-axes lie within the sample plane with an accuracy of about 1.0 degree. As shown in Fig. 1b, no extra reflections were observed, indicating that the crystal is free of mosaic block structures.

3.2. Temperature-Dependent Susceptibility

Figure 2 displays the zero-field-cooled (ZFC) and field-cooled (FC) magnetization $M(T)$ in μ_B/f.u. units for $\mu_0 H = 0.01\,\mathrm{T}$ and $\mu_0 H = 0.1\,\mathrm{T}$ applied along the three principal axes. All curves exhibit a pronounced "kink" at $T_\mathrm{N} \approx 32\,\mathrm{K}$, signalling the onset of ferrimagnetic order arising from two different magnetic sublattices. A second "kink" occurs at $T_\mathrm{kink} \approx 21\,\mathrm{K}$.

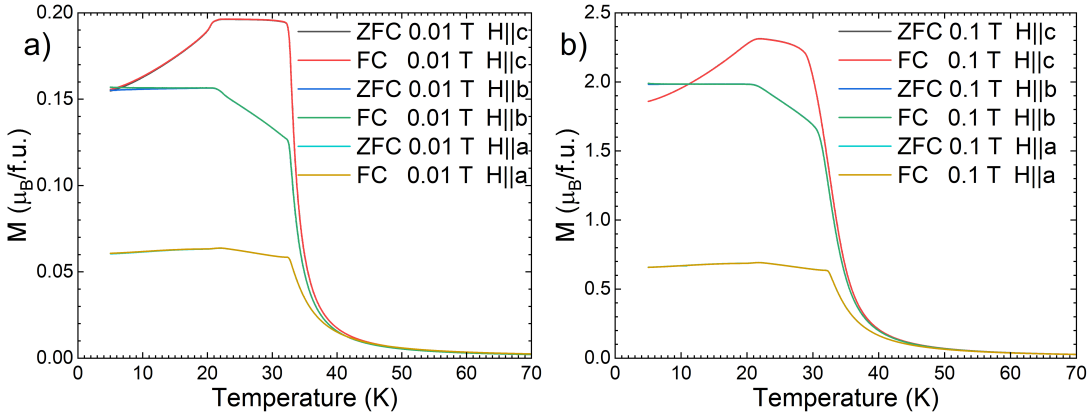

Figure 2. ZFC/FC magnetization $M(T)$ for (a) $B = 0.01\,\mathrm{T}$ and (b) $B = 0.1\,\mathrm{T}$ applied along the three principal axes.

The high-temperature ($T > 45\,\mathrm{K}$) susceptibility follows a Curie–Weiss law:

$$\chi(T) = \frac{C}{T - \theta_\mathrm{CW}} + \chi_0, \tag{1}$$

where C is the Curie constant, θ_CW is the Curie–Weiss temperature, and χ_0 is the temperature-independent contribution. We find effective moments $\mu_\mathrm{eff} \approx 6.62, 6.05, 6.28\,\mu_B$ and Curie–Weiss temperatures $\theta_\mathrm{CW} \approx 34.3, 35.5, 35.7\,\mathrm{K}$ for $H \parallel a, b, c$ axes, respectively. A positive θ_CW value in a ferrimagnetic crystal results from a combination of antiferromagnetic interactions between the Gd and Ti magnetic sublattices, as well as ferromagnetic coupling within each sublattice. Temperature-independent contribution is isotropic and equals to $-0.0000029\,\mu_\mathrm{B}$ per f.u. and originates from sample holder of VSM option.

A clear magnetic anisotropy emerges below T_N, with the magnetization ordering $M_c > M_b > M_a$, reflecting a complex interplay of magnetic interactions. The ZFC/FC splitting is negligible for all measured directions, with the splitting most pronounced for $H \parallel b$ at low temperatures below 10 K. The magnified ZFC-FC splitting along the b axis suggests the presence of energy barriers that impede magnetic moment reorientation and domain wall motion during the cooling process without an external field. In contrast, the field-cooled measurement, performed under

applied magnetic field, allows partial alignment of magnetic moments despite these pinning constraints. The resulting divergence between ZFC and FC data is a signature manifestation of anisotropic magnetic interactions and structural or magnetic pinning centers that preferentially couple to magnetic moments oriented along the b axis.

3.3. Isothermal Magnetization

Representative $M(H)$ loops measured at 5 K and 25 K for all three crystallographic axes are shown in Figure 3 for the first quadrant. For all directions the loop exhibits slight hysteresis ($\mu_0 H_c \approx 5$ mT) and nearly complete saturation in the field range $\mu_0 H_{\text{sat}} \approx 0.3$–$0.5$ T ($H \parallel c$ and $H \parallel b$ axes) and $\mu_0 H_{\text{sat}} \approx 0.9$–$1.1$ T ($H \parallel a$ axis). Beyond these field ranges the magnetization increases gradually up to saturation at $M_{\text{sat}} \approx 6.08\,\mu_B$ f.u.$^{-1}$ at 9 T for $H \parallel c$ and $\approx 6.05\,\mu_B$ at 9 T for $H \parallel b$ and a axes.

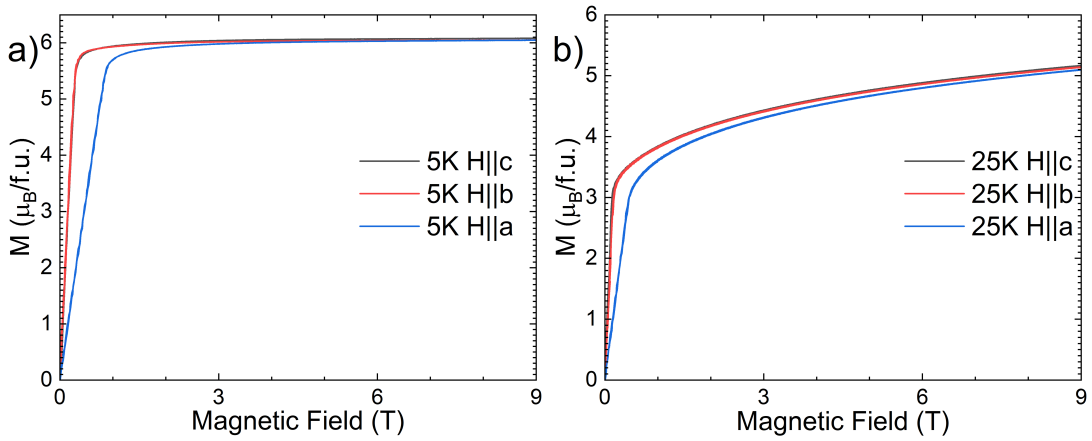

Figure 3. Isothermal magnetization $M(H)$ at (a) $T = 5$ K and (b) $T = 25$ K within the applied magnetic field, $\mu_0 H$, range of 0–9 T applied along the three principal axes.

From the isothermal magnetization curves, an easy-plane behavior in the bc plane is observed. The temperature raise within 5–25 K does not change the behaviour significantly.

From the data one could see that saturated magnetic moment per formula unit (approximately $6\,\mu_B$) can be explained as two magnetic sublattices of Gd^{3+} ($7\,\mu_B$, $4f^7$) and Ti^{3+} ($1\,\mu_B$, $3d^1$) that align antiferromagnetically below the critical temperature T_N, thus confirming ferrimagnetic ordering.

4. Discussion

4.1. Origin of Magnetic Anisotropy

Temperature-dependent magnetization $M(T)$ below the Neel temperature T_N shows significant differences between $H \parallel c$, $H \parallel b$ and $H \parallel a$ directions in low fields, with a pronounced secondary transition at $T_{\text{kink}} = 21$ K. However, high-field $M(H)$ measurements show that magnetization curves for both orientations ($H \parallel c$ and $H \parallel b$) nearly coincide. This discrepancy reflects the complex interplay of magnetic anisotropy contributions that change with temperature and applied field.

The experimental data clearly establish that the magnetic easy plane lies within the bc crystallographic plane. This planar anisotropy originates from multiple sources: anisotropic spin-spin interactions [21] within and between the Gd and Ti sublattices, spin-orbit coupling from Gd $4f^7$ electrons, and crystal field splitting of the Gd^{3+} ^8S [22] and Ti^{3+} ^2D states. Strong

applied fields effectively overcome these anisotropic contributions, explaining the field-dependent behavior.

The orthorhombic distortion of $GdTiO_3$ creates asymmetric Ti-O-Ti superexchange pathways. The Ti-O-Ti bond angle is approximately 145.5° along the *b* axis but 147° in the *ac* plane. According to the Goodenough-Kanamori-Anderson (GKA) rules, this difference results in weaker superexchange along *b* axis compared to the *ac* plane, establishing anisotropy within the Ti^{3+} sublattice.

Beyond Ti-O-Ti superexchange, Gd-O-Ti and Gd-O-Gd pathways also contribute significantly. Quantitative understanding of these competing contributions requires density functional theory calculations to evaluate exchange parameters, crystal field splittings, and magnetic anisotropy constants as functions of temperature and field.

4.2. Implications for Spintronic Applications

The sizable anisotropic coercivity suggest that $GdTiO_3$ could serve as a functional layer in heterostructures where magnetic orientation must be controlled by modest external fields. Moreover, the strong coupling between the 4f and 3d moments may enable electric field manipulation of magnetism in $GdTiO_3$-based oxide interfaces, an avenue worth exploring in future work.

5. Conclusions

High quality $GdTiO_3$ single crystal were grown by the optical floating zone method and characterized structurally by X ray diffraction.

Magnetization measurements reveal a pronounced magnetic anisotropy: the Neel temperature is isotropic ($T_N \approx 32$ K), whereas the magnetization depend strongly on the field direction.

These findings deepen our understanding of spin orbital coupling in rare earth titanates and provide a solid experimental basis for theoretical modelling of anisotropic magnetism in correlated oxides and for further development of solid-state cryogenic coolers based on the magnetocaloric effect for solving the problem of hydrogen liquefaction.

Acknowledgments

The study was supported by a grant from the Russian Science Foundation No. 25-22-00324.

References

1. Turner C. W., Greedan J. E., *Journal of Solid State Chemistry* **34**, 207 (1980).

2. Disa A. S., Curtis J., Fechner M., Liu A., von Hoegen A., Först M., Nova T. F., Narang P., Maljuk A., Boris A. V., Keimer B., Cavalleri A., *Nature* **617**, 73 (2023).

3. Najev A., Pocrnic M., Barisic D., Vojta M., Kuzmin M., et al., *Physical Review B* **109**, 174406 (2024).

4. Grisolia M. N., Bruno F. Y., Sando D., Zhao H. J., Jacquet E., Chen X. M., Bellaiche L., Barthélémy A., Bibes M., *Applied Physics Letters* **105**, 172402 (2014).

5. Omote H., Watanabe S., Matsumoto K., Gilmutdinov I., Kiiamov A., Tayurskii D., *Cryogenics* **101**, 58 (2019).

6. Zhang J. Y., Jackson C. A., Chen R., Raghavan S., Moetakef P., Balents L., Stemmer S., *Physical Review B* **88**, 121104(R) (2013).

7. Yang L. J., Wang H. Y., Wang Y. K., Wan X. G., *Journal of Physics: Condensed Matter* **26**, 476001 (2014).

8. Khalsa G., Benedek N. A., Moses J., *npj Quantum Materials* **3**, 15 (2018).

9. Mochizuki M., Imada M., *Journal of the Physical Society of Japan* **73**, 1833 (2004).

10. Goodenough J. B., *Journal of Materials Chemistry* **17**, 2394 (2007).

11. Amow G., Zhou J. S., *Journal of Solid State Chemistry* **154**, 447 (2000).

12. Hameed S., Barone D., Mehio O., Sr. D. H., Frandsen B., Balents L., Wilson S. D., *Physical Review Materials* **5**, 125003 (2021).

13. Sergienko I. A., Dagotto E., *Physical Review B* **73**, 094434 (2006).

14. Craco L., Laad M. S., Leoni S., Müller-Hartmann E., *Physical Review B* **77**, 075108 (2008).

15. Need R. F., Isaac B. J., Kirby B. J., Borchers J. A., Stemmer S., Wilson S. D., *Physical Review Letters* **117**, 037205 (2016).

16. Garcia-Barriocanal J., Cezar J. C., Bruno F. Y., Thakur P., Brookes N. B., Utfeld C., Rivera-Calzada A., Giblin S. R., Taylor J. W., Duffy J. A., Dugdale S. B., Nakamura T., Kodama K., Leon C., Okamoto S., Santamaria J., *Nature Communications* **1**, 82 (2010).

17. Suzuki T., Yamauchi I., Udagawa M., Goto M., *Physica B: Condensed Matter* **329–333**, 943 (2003).

18. Nabokin P. I., Souptel D., Balbashov A. M., *Journal of Crystal Growth* **250**, 397 (2003).

19. Zhou H. D., Goodenough J. B., *Physical Review B* **72**, 045125 (2005).

20. Turner C. W., Greedan J. E., *Journal of Magnetism and Magnetic Materials* **38**, 29 (1983).

21. Leushin A., Eremin M., *J. Exp. Theor. Phys* **69**, 2190 (1975).

22. Eremin M., Antonova I., *Journal of Physics: Condensed Matter* **10**, 5567 (1998).